EUV IMAGING SPECTROMETER
Hinode

EIS SOFTWARE NOTE No. 2

Version 0.8 9 March 2010

EIS RADIOMETRIC CALIBRATION

John Mariska
Code 7673
Naval Research Laboratory
Washington, DC 20375
USA

John.Mariska@nrl.navy.mil

1 Overview

This document outlines the factors that went into determining the prefilight radiometric calibration of EIS and discusses the sensitivity changes that have taken place since Hinode was launched.

2 Preflight Calibration Information

EIS consists of a multilayer-coated, normal-incidence off-axis telescope and a normal-incidence, toroidal-grating, stigmatic spectrometer covering two wavelength bands in the EUV. Figure 1 shows the basic EIS optical layout.

The performance of each optical element was characterized before the final instrument was assembled. The following sections summarize the results of that work. In §3 all the information is combined to create the EIS effective area curves.

2.1 Front Filter and Spectrometer Entrance Filter

To reject visible light, EIS has two 1500 Å thick Al filters in the optical path. The front filters are mounted in four filter frames and protected by a clamshell that can be evacuated for launch. The spectrometer entrance filter is located on a structure bulkhead just past the slit mechanism. All the filters sit on a mesh with an estimated transmission of 0.85.

All the candidate filters were measured at Brookhaven, and flight filters and spares were then selected. Figure 2 shows the measured filter transmission curves. For comparison, the figures also

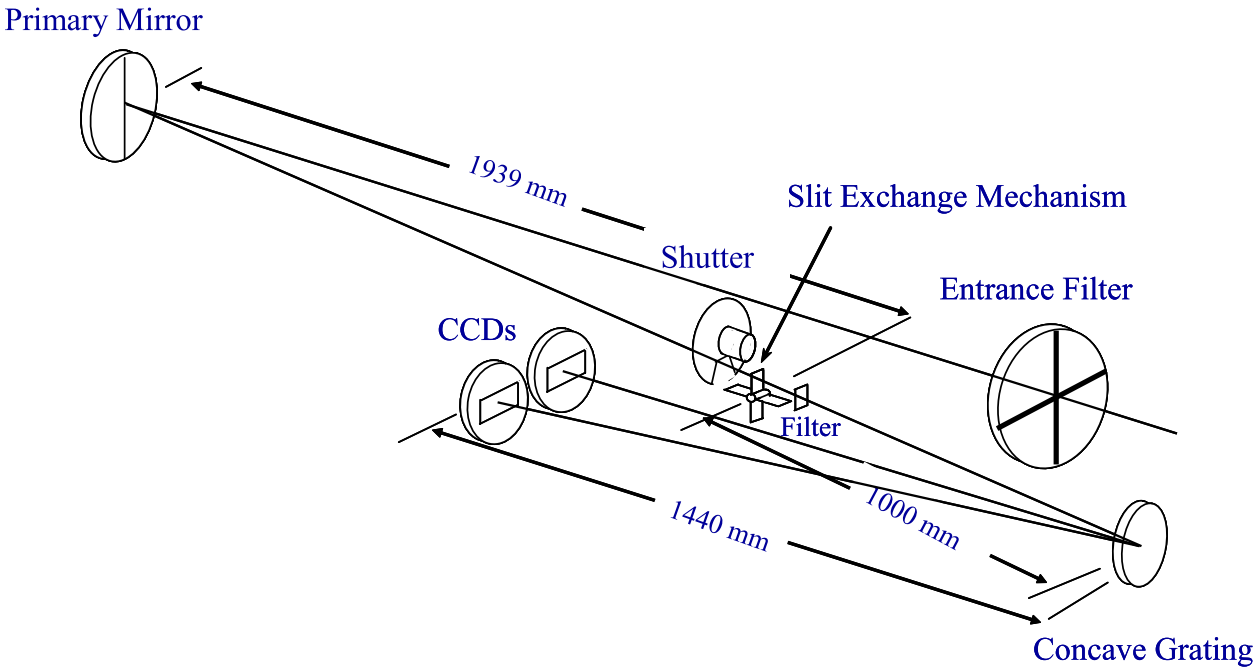

Figure 1: EIS optical diagram.

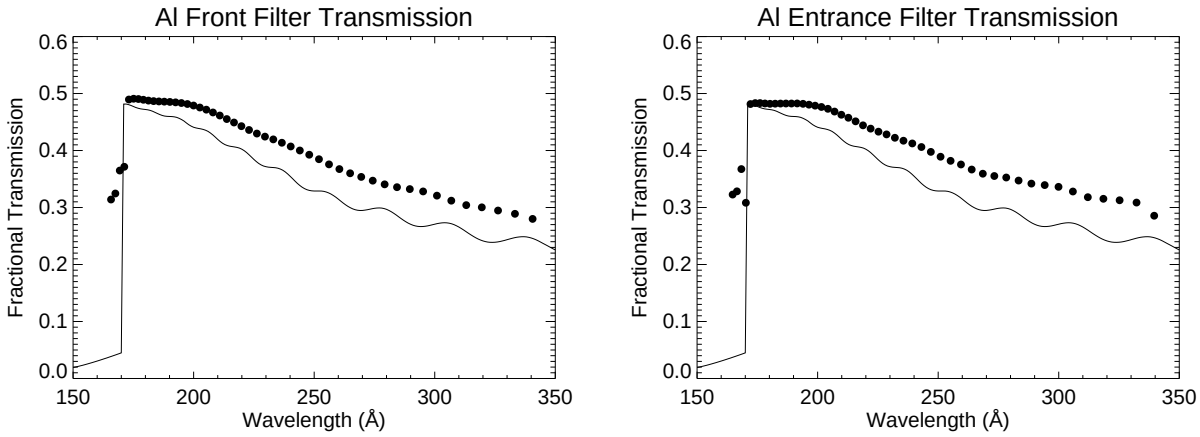

Figure 2: Measured transmissions for one of the the Al front filters (SN 10) and the flight spectrometer entrance filter. The solid lines are the theoretical transmission curves that were used for earlier calculations multiplied by a factor of 0.85 to account for the transmission of the filter mesh.

show the theoretical data that were used earlier during instrument development. Note that the measured transmission curves automatically include the mesh transmission factor that was carried separately in some earlier calculations of the EIS effective areas.

The filter transmission data are contained in the files `EIS_FFATrans.002` and `EIS_SEFTrans.002` in the directory `$SSW/hinode/eis/response`, where `$SSW` is the path to the beginning of the software in the SSW system.

2.2 Mirror

The EIS flight mirror (SN-1) if an off-axis paraboloid with a clear aperture of 150 mm, a focal length, f, of 1938.68 mm, and an off-axis distance to center of 145.5 mm (Reference is Tinsley Laboratories sheet accompanying the mirror).

A multilayer coating was applied to each half of the mirror by Dave Windt. These were then measured at Brookhaven by John Seely, who provided a detailed report and reflectance curves as a function of wavelength for each half of the mirror. Figure 3 shows the measured reflectivities for the flight mirror. The reflectances are contained in the files `EIS_MirrorRefl_A.003` and `EIS_MirrorRefl_B.003` in the directory `$SSW/hionde/eis/response`, where `$SSW` is the path to the beginning of the SSW software system.

The EIS mirror mechanism has both coarse movement and fine scan capability. For coarse movement—to change the position of the Sun relative to the other instruments—the mirror is shifted in the $\pm X$-direction. The mirror travels ± 10 mm in its coarse motion. This motion changes the portions of the mirror that are obstructed by the support spider in the front filter assembly. The narrow segments of the spider are 10.5 mm wide, so as the mirror travels, one side increases in area while the other decreases. Once the travel reaches 5.25 mm, this ceases and one side loses area and the other remains about constant since the opposite coating starts to appear from under the spider. This is illustrated in the left side of Figure 4.

A small amount of vignetting due to obstruction by the doghouse surrounding the CCDs is also

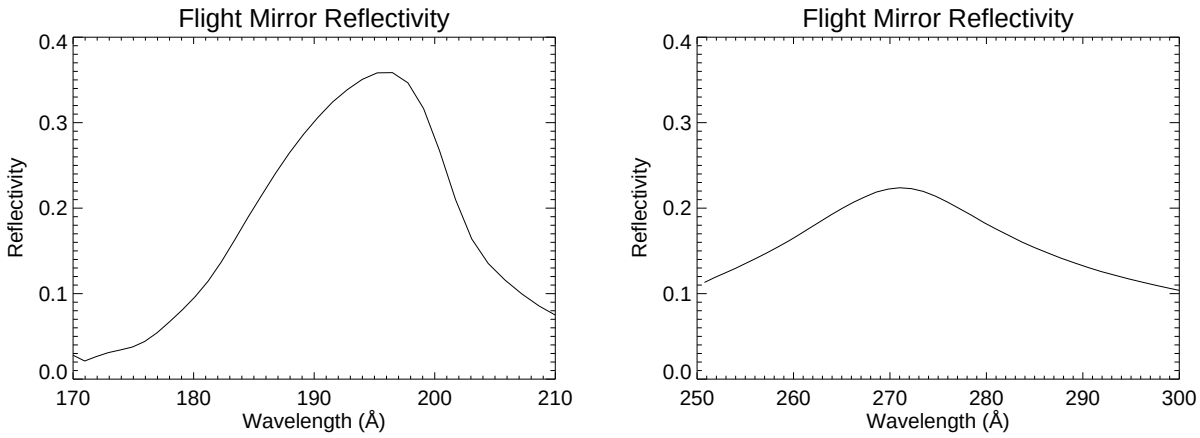

Figure 3: Measured reflectivities for the short and long wavelength bands on the EIS flight mirror.

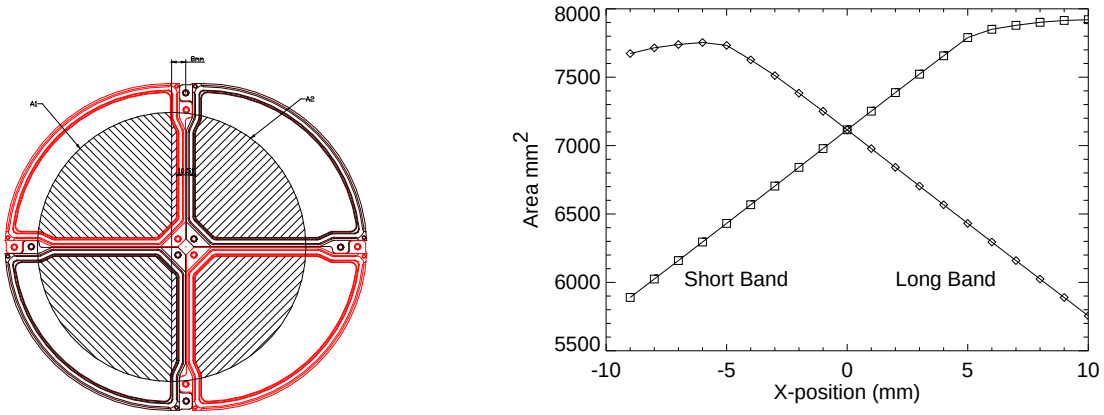

Figure 4: Left side: EIS mirror displaced by coarse movement behind the spider. Right side: EIS mirror area as a function of the coarse X-position.

Table 1: EIS Mirror Area for Changing X-positions

X mm	A1 mm^2	A2 mm^2	Doghouse mm^2	SW Area mm^2	LW Area mm^2
10	5755.4	7920.7		7920.7	5755.4
9	5889.7	7914.9		7914.9	5889.7
8	6024.4	7901.4		7901.4	6024.4
7	6159.6	7879.2		7879.2	6159.6
6	6295.2	7850.4		7850.4	6295.2
5	6431.2	7790.0		7790.0	6431.2
4	6567.5	7656.6		7656.6	6567.5
3	6704.2	7522.4		7522.4	6704.2
2	6841.1	7387.5		7387.5	6841.1
1	6978.3	7251.7		7251.7	6978.3
0	7115.3	7115.3		7115.3	7115.3
−1	7251.7	6978.3	−0.86	6978.3	7250.8
−2	7387.5	6841.1	−4.32	6841.1	7383.2
−3	7522.4	6704.2	−10.6	6704.2	7511.8
−4	7656.6	6567.5	−29.3	6567.5	7627.3
−5	7790.0	6431.2	−57.3	6431.2	7732.7
−6	7850.4	6295.2	−96.4	6295.2	7754.0
−7	7879.2	6159.6	−140.0	6159.6	7739.2
−8	7901.4	6024.4	−186.6	6024.4	7714.8
−9	7914.9	5889.7	−241.9	5889.7	7673.0

found in the long wavelength band as the mirror moves toward $-X$. Charlie Brown has calculated all the vignetting on the telescope side of EIS. Table 1 and the plot on the right side of Figure 4 summarizes these calculations. These area changes are not currently included in any calculations of the EIS effective area. Instead, the mirror area of 8835.7 mm^2 is reduced by a spider transmission factor of 0.8.

The position of the mirror in its coarse motion is measured with a resolver that has a range from 0x4195 at the $-X$ limit to 0x1408 at the $+X$ limit with a wraparound at 0xFFFF, i.e., 0xFFFF, 0, 1 to $-X$. Travel from the $+X$ direction toward the $-X$ direction is denoted as the forward direction. The resolver numbers are twos-complement. The relationship between the resolver measurement and the position of the mirror has been measured. The relationship between the current position of the mechanism and the table has not been determined.

2.3 Slit/Slot

The EIS slits were fabricated using a Si substrate and a photolithography process. Slit widths were measured at the left center and right side of each slit. Average values for the widths in μm of the flight slits are 9.3, 19.2, 384, and 2507 for the 1, 2, 40, and 266 arcsec slits, respectively.

The slits are attached to a four vaned paddlewheel located immediately behind the shutter. It is possible to move the slit/slot mechanism in either the forward or reverse direction. To avoid damage with time, however, NRL and Perdix recommended that the mechanism only be moved in the forward direction (vane through which sunlight passes moves toward the grating). The order

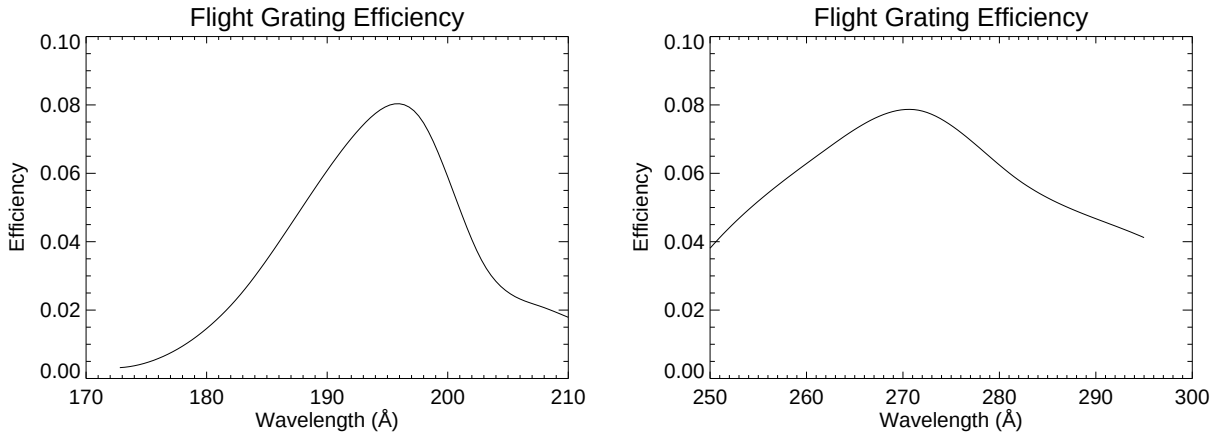

Figure 5: Measured efficiencies for the short and long wavelength bands on the EIS flight grating.

of the slits on the mechanism is 1 arcsec, 266 arcsec, 2 arcsec, and 40 arcsec. The slit/slot disk rotates at a rate of 20 ms per step and a 90° rotation takes 324 steps. Thus, it takes 6.48 s for a 90° rotation of the mechanism.

2.4 Grating

The EIS flight grating comes from a family of toroidal gratings fabricated by Zeiss. The flight candidate gratings were ruled with 4200 l/mm and a multilayer coating was applied to each half by Dave Windt. The gratings were then measured at Brookhaven. Details of the various measurements that were carried out on the grating are contained in a series of documents by John Seely and others on the NRL team. Figure 5 shows the resulting grating efficiencies (a combination of the multilayer reflectivities and the groove efficiency) for the current flight grating (FL-7). The measured efficiencies are contained in the files `EIS_GratingRefl_A.003` and `EIS_GratingRefl_B.003` in the directory `$SSW/hinode/eis/response`, where `$SSW` is the path to the beginning of the SSW software system.

Due to the tight clearances between the slit/slot assembly and the light beams from the EIS mirror, it was necessary to accept some vignetting at the long wavelength end of the long wavelength band detector by the doghouse enclosure that keeps the slit/slot assembly light tight. This amount of vignetting has been computed by Charlie Brown. Figure 6 shows a plot of the vignetting factor for the case where the EIS mirror coarse motion is at the zero position along with a table of values. The numbers used to generate the figure are contained in the file `EIS_vignetting.001` in the directory `$SSW/hinode/eis/response`, where `$SSW` is the path to the SSW software system. These factors are used in computing the EIS effective area for the long wavelength band.

2.5 Camera

The EIS camera contains two Marconi 42-20 back-illuminated CCDs with 2048 pixels in the dispersion direction and 1024 pixels in the spatial direction. In both directions, the pixel size is 13.5 μm. In the dispersion direction, the CCDs have 50 lead-in pixels at each end of the serial register. Data

Wave	Vignetting Factor
270.0	1.000
272.0	1.000
274.0	1.000
276.0	0.993
278.0	0.966
280.0	0.920
282.0	0.865
284.0	0.804
286.0	0.738
288.0	0.667
290.0	0.596

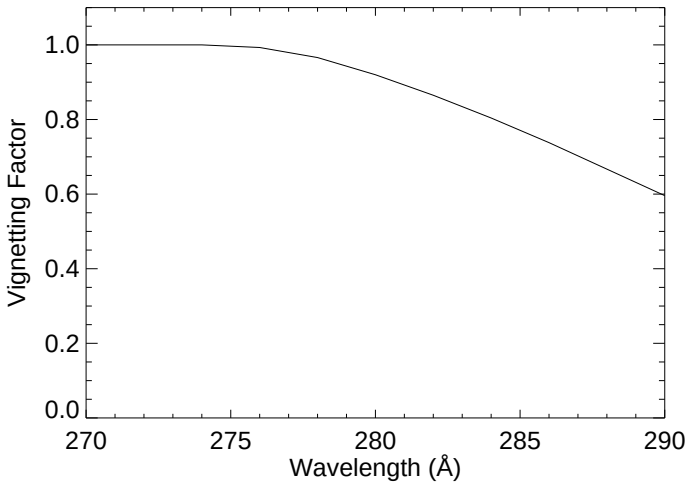

Figure 6: Vignetting factor due to doghouse.

from the testing and calibration at RAL has those pixels included. (This may in the future lead to some confusion about pixel numbering in the dispersion direction.) The read time for the CCD is 0.8 s.

Engineering models of the CCDs were measured at Brookhaven. For one CCD (EM443-02-07), the average quantum efficiencies at 190 and 270 Å, were 0.61 and 0.57, respectively. For the other CCD (EM443-01-04), the corresponding values were 0.52 and 0.48. After looking at additional information it has been agreed within the EIS MSSL team that we will use a constant QE of 0.64.

The EIS camera operates in an integrating mode. The shutter is opened for a short interval and photon events are summed into the CCD pixels. Thus the amount of charge read out of the CCD by the camera provides a measure of the energy that has been integrated in each pixel and not the actual number of photons counted. Since EIS is a spectrometer, however, when the 1 or 2 arcsec slit is used, the photons striking each pixel are essentially monoenergetic, and the amount of accumulated charge is directly proportional to the photon flux.

EUV photons striking the CCD produce electron-hole pairs in the silicon. It takes 3.65 eV to produce an electron-hole pair, so the number of electrons produced by a photon of wavelength λ (Å) is given by

$$N_{e^-} = \frac{12398.5}{\lambda} \times \frac{1}{3.65} \ . \tag{1}$$

Thus, at 195 Å, one photon produces 17.4 electrons, at 270 Å, one photon produces 12.6 electrons, and at 290 Å—the longest wavelength covered by the spectrometer—one photon produces 11.7 electrons. The EIS CCDs have a full-well capacity of about 90,000 electrons.

The charge accumulated in each pixel is converted by 14-bit analog-to-digital converters into data numbers (DN) using the expression

$$\mathrm{DN} = N_{e^-}/G + \mathrm{offset} \ , \tag{2}$$

where G is the gain and a digital offset is added. The value of G is currently measured to be 6.93 electrons DN^{-1}. Current values of the offset seem to be between 500 and 550 DN depending on which CCD and which port the data are read from.

In addition to the photon-shot noise, the EIS camera has quantization and readout noise. The design criteria for the EIS camera called for it to have a total signal chain noise comparable to the photon noise, leading to a requirement for a total noise level of 10 electrons RMS. For the lowest signal levels, this puts the camera noise just below the shot noise for a photon at 290 Å. Measurements of the flight model camera show that the noise level is in the range 10.1 to 13.5 electrons. With the value of G set to 5.65, this corresponds to 1.8 to 2.4 DN.

3 EIS Effective Areas

For an ideal optical system with no losses, the number of photons of wavelength λ entering the slit per second in a height interval corresponding to one pixel in the spatial dimension on each CCD, $N_\lambda^{\rm slit}$, is given by

$$N_\lambda^{\rm slit} = \phi_\lambda A \frac{a}{f^2}, \tag{3}$$

where, ϕ (photons cm^{-2} s^{-1} sr^{-1}) is the intensity of the solar radiation, A (cm^2) is the mirror area, a (cm^2) is the area of the slit corresponding to one spatial CCD pixel in height times the width of slit, and f is the focal length of the mirror. These photons are then imaged onto the CCD in a manner determined by the magnification in the spectrograph section of the instrument. Thus, the number of photons per second registered on a pixel of each CCD is given by

$$N_\lambda = \phi_\lambda A \frac{a}{f^2} \frac{1}{n_{\rm pix}}, \tag{4}$$

where the division by $n_{\rm pix}$ provides the desired solid angle per detector pixel. The design goal was to have the narrow slit match the pixel size. But the actual slit widths result in small corrections. For the narrow slit (nominally 1 arcsec wide), $n_{\rm pix}$ is 1.067 and 1.087 for detectors A and B, respectively. The corresponding values for the 2 arcsec slit are 2.080 and 2.119. Note that the combination of factors results in the same solid angle per detector pixel, $\omega_{\rm d}$.

Of course, EIS is not an ideal optical system. The actual number of registered photons will be reduced by additional factors due to the transmission of the two aluminum filters, the reflectivity of the mirror, the efficiency of the grating, and the quantum efficiency of the detectors. Thus, the basic expression for the number of photons registered in each detector pixel per second is

$$N_\lambda = \phi_\lambda A \omega_{\rm d} T_{\rm ffa}(\lambda) T_{\rm spider} R_{\rm m}(\lambda) E_{\rm g}(\lambda) V_{\rm d}(\lambda) T_{\rm sef}(\lambda) E_{\rm d}(\lambda), \tag{5}$$

where $T_{\rm ffa}(\lambda)$ and $T_{\rm sef}(\lambda)$ are the transmissions of the aluminum front filter assembly and spectrometer entrance filter, respectively; $T_{\rm spider}$ is the transmission of the spider that is part of the front filter assembly; $R_{\rm m}(\lambda)$ is the reflectivity of the mirror coatings; $E_{\rm g}(\lambda)$ is the grating efficiency, which includes both the groove efficiency and the reflectivity of the multi-layer coatings, $V_{\rm d}(\lambda)$ is is a vignetting factor to account for the vignetting at the long wavelength end of the long wavelength detector; and $E_{\rm d}(\lambda)$ is the detector quantum efficiency. Note that the Al filter transmission factors are a combination of the transmission of the thin Al material and a factor $T_{\rm mesh}$, the transmission of the mesh that supports both aluminum filters. This value, estimated to be 0.85, was carried separately in early calculations of the EIS sensitivity, but is now included in the measured filter data.

All the factors apart from the solid angle are often grouped into an effective area $A_{\rm eff}(\lambda)$, leading to the expression

$$N_\lambda = \phi_\lambda A_{\rm eff}(\lambda) \omega_{\rm d}. \tag{6}$$

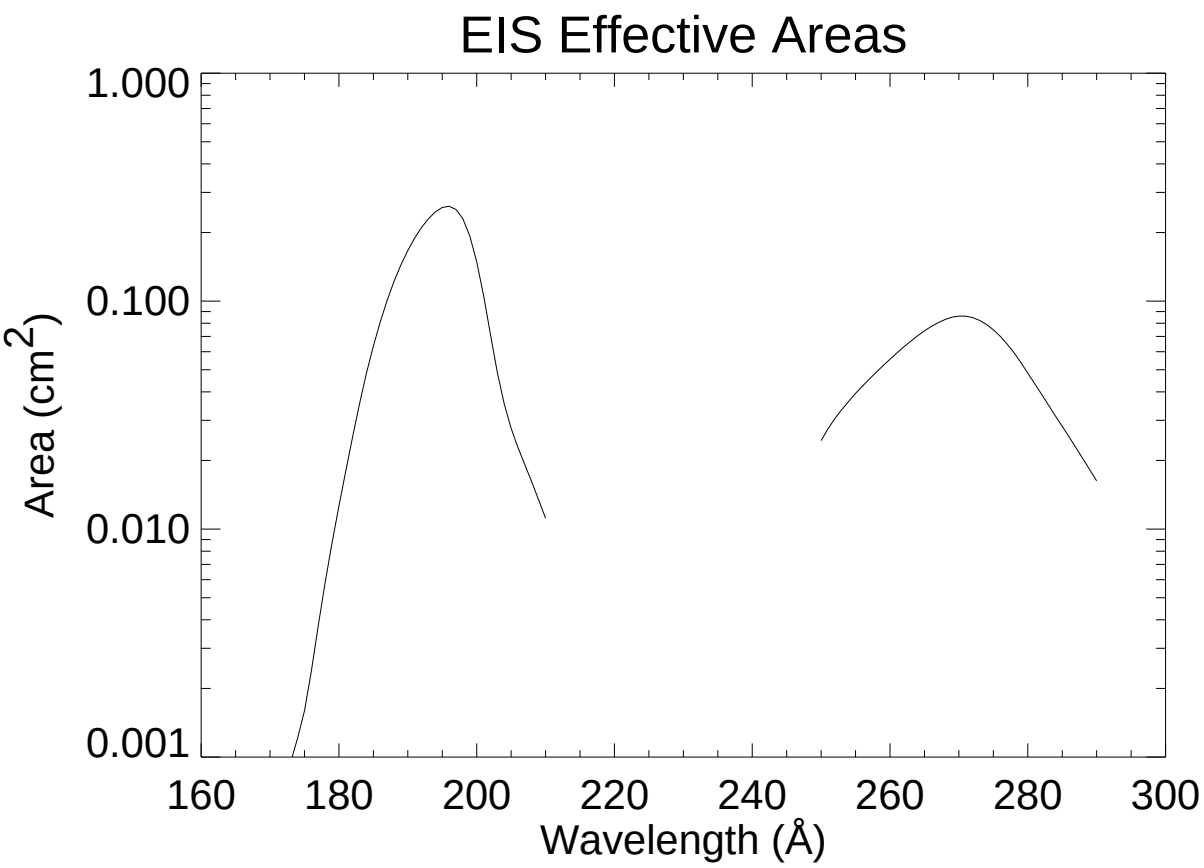

Figure 7: EIS effective areas.

Figure 7 shows the effective areas for the two EIS wavelength bands.

4 EIS Radiometric Calibration at RAL

5 EIS Sensitivity Changes on Orbit

In December 2006, NRL initiated a program of regular observations of quiet Sun regions near Sun center to monitor EIS sensitivity changes. The initial studies, SYNOP001 and SYNOP002 took exposures covering all the wavelengths covered by the CCDs. After the X-band transmitter failure early in 2008, these were replaced with studies that only covered selected emission lines (SYNOP005_A and SYNOP006).